Surfaces and Interfaces 38 (2023) 102778

Contents lists available at ScienceDirect

Surfaces and Interfaces

journal homepage: www.sciencedirect.com/journal/surfaces-and-interfaces

Antimicrobial activity of porous metal injection molded (MIM) 316L stainless steel by Zn, Cu and Ag electrodeposition

Matti Kultamaa [a], Marianne Gunell [b,c], Kari Mönkkönen [d], Mika Suvanto [a,*], Jarkko J. Saarinen [a,*]

[a] Department of Chemistry, University of Eastern Finland, P.O. Box 111, FI-80101 Joensuu, Finland
[b] Department of Clinical Microbiology, Turku University Hospital, 20521 Turku, Finland
[c] Department of Medical Microbiology and Immunology, University of Turku, 20500 Turku, Finland
[d] Karelia University of Applied Sciences, FI-80200 Joensuu, Finland

ARTICLE INFO

Keywords:
Metal injection molding (MIM)
Stainless steel 316L
Porous metal
Electrodeposition
Antimicrobial activity
Staphylococcus aureus

ABSTRACT

Porous 316L stainless steel samples were functionalized with electrodeposited zinc, copper, and silver coatings for antimicrobial activity against gram-positive bacteria *Staphylococcus aureus* (*S. aureus*). Porous stainless steel samples were created by combining metal injection molding (MIM) with a powder space holder (PSH) technique using sodium chloride (20 wt%) as a space holder material. Galvanostatic (0.10 A) electrodeposition was used for zinc, copper, and silver deposition, and antimicrobial activity of functionalized samples was evaluated using a touch test protocol with *S. aureus*. All electrodeposited samples completely prevented the growth of *S. aureus*. These results confirm that metal depositions only in the pores of the porous 316L were sufficient to inhibit the growth of *S. aureus* completely.

1. Introduction

Austenitic 316L stainless steel is a widely used metal with multiple suitable properties such as low cost, good mechanical strength, simplicity of fabrication, and decent corrosion resistance [1–3]. Therefore, 316L is used, for example, in nuclear reactors, marine applications, and hydraulic components [1,4]. Another important field of application for 316L stainless steel is medical industry, where it is used in biomedical implants and surgical instruments [1,3,5]. However, a wide scale utilization of 316L in medical field is limited by low biocompatibility, which manifests as a release of harmful ions such as nickel and chromium when in contact with bodily fluids in physiological environment [2,3,5]. This can lead to adverse inflammatory and allergic reactions or even cancer [3,5]. Another important limiting factor for a wide use of 316L stainless steel in medical applications is its poor antimicrobial activity [3].

Materials with antimicrobial properties are of paramount importance in hospitals and healthcare centers. Healthcare-associated infections (HAIs) can be transmitted not only from invasive devices and surgical instruments but also from commonplace items such as furniture, door knobs, and trays [6,7]. Attachment of pathogens onto a surface can lead to a formation of a biofilm i.e. an accumulated microbial community on a surface [6,8,9]. Biofilms formed by infectious pathogens are difficult to remove as the biofilm offers an added resistance to antibiotics and common disinfectants for the bacterial species [3,6,8,10,11]. Thus, an optimal way to prevent bacterial biofilm growth is to inhibit their formation and growth by surface modification and antimicrobial coatings [3,6,10–12].

Austenitic stainless steels including 316L are used as orthopedic implants [5]. However, 316L has a significantly larger Young's modulus than the surrounding bone [13] that may result in loosening of the 316L implant [13,14]. This difference in Young's modulus can be reduced by fabricating the implant from porous stainless steel [5,14]. Sufficiently interconnected porosity may also promote bone ingrowth into the porous metal material improving the attachment of the implant [14].

Metal injection molding (MIM) is a relatively new fabrication method, which allows formation of porous stainless steels when coupled with powder space holder (PSH) technique. In PSH-MIM, space holder material is mixed with the MIM feedstock that is subsequently molded, debinded and sintered. The space holder material is removed during debinding from the metal structure leaving behind pores, which remain in the structure during the consolidation process by sintering. Poly

* Corresponding authors.
E-mail addresses: mika.suvanto@uef.fi (M. Suvanto), jarkko.j.saarinen@uef.fi (J.J. Saarinen).

https://doi.org/10.1016/j.surfin.2023.102778
Received 4 March 2022; Received in revised form 25 January 2023; Accepted 26 February 2023
Available online 1 March 2023

(methylmetacrylate) (PMMA) has been demonstrated as a feasible space holder material in the fabrication of porous 316L stainless steel [15–17].

Antimicrobial activity of stainless steels used in medical environments has been improved by electrochemically applied coatings on stainless steel surface. In this study, zinc, copper, and silver electrodeposition was used to improve the antimicrobial activity of porous 316L stainless steel. The antimicrobial properties of these three metals are well-known [18]. Cyanide based baths have traditionally been used for the silver, zinc, and copper electrodeposition, while the latter two are also commercially electroplated from chloride and sulfate based baths, respectively [19–21]. Recently, electrodeposited composite coatings consisting of Zn/Ag particles, Cr/Ag nanoparticles, and Zn-Cu/silver nanoparticles were used for improved antibacterial activity [22–24].

Applying an antimicrobial metal coating on a porous 316L stainless steel can extend applicability of 316L in medical industry. Although the antimicrobial activity of 3D printed porous 316L stainless steel was recently reported by silver incorporated zeolite coatings [25], the topic has not been thoroughly investigated so far.

The objective of this study was to improve the antimicrobial activity of porous injection molded 316L stainless steel by electrodeposition. Porous 316L specimens were fabricated using the PSH technique with 20 wt% NaCl as an environmentally friendly space holder material. Galvanostatic electrodeposition of zinc, copper, and silver was utilized to improve the antimicrobial activity of porous 316L stainless steel. Gram-positive *Staphylococcus aureus* (*S. aureus*), which is one of the most common causes of HAIs, was used as a test bacterial species in the bacterial touch tests mimicking bacterial transfer from surfaces. Our results demonstrate that porous 316L stainless steel can be functionalized with deposition of antimicrobial metals into the pores for improved antimicrobial activity of stainless steel.

2. Materials and methods

2.1. Metal injection molding (MIM)

Austenitic polyMIM® 316L D 120E stainless steel MIM feedstock material (polyMIM GmbH, Bad Sobernheim, Germany) was used in metal injection molding. The main constituent of the feedstock material is iron, and the typical additive levels as provided by the manufacturer are shown in Table 1. In fabrication of porous specimens, sodium chloride (Hankkija Oy, Hyvinkää, Finland) was used as space holder material. Porosity level was controlled by NaCl content and was set to 20 wt%.

Granular 316L stainless steel and NaCl with particle sizes of 0.3–8.0 mm was milled separately using an Ultra Centrifugal Mill ZM 200 (Retsch GmbH, Haan, Germany) with a 1.5 mm ring sieve. Rotor speeds of 10,000 rpm and 6000 rpm were used, respectively. Milled NaCl was sieved with a Vibratory sieve shaker AS 200 digit (Retsch GmbH, Haan, Germany) to limit the NaCl crystal sizes to 200–315 μm. The particle size of space holder material determines the pore size in the final sintered product.

Both 316L and NaCl were milled to ensure a thorough mixing of these two materials prior to injection molding. Manual mixing was employed, and 1.0 wt% paraffin wax (VWR Chemicals BDH, Leuven, Belgium) was added to increase flowability of the mixture during injection molding.

HAAKE MiniJet II injection molding system (Thermo Fisher Scientific, Karlsruhe, Germany) was used in MIM. Cylinder temperature of 190 °C, mold temperature of 60 °C, pressure of 450 bar, and injection time of 3 s were used. The fabricated samples had a cylindrical, coin-like shape with final sintered diameter of 20.9 mm and thickness of 5.1 mm.

After injection molding, the samples (called green parts) were subjected to solvent debinding, in which NaCl and the water-soluble part of the binder material incorporated in the 316L feedstock were removed from the samples. Debinding was carried out in a deionized water bath at 60 °C for a minimum of 48 h. Debinded samples (called brown parts) were dried in an oven at 100 °C for 2 h. The samples were weighed before and after debinding to guarantee complete removal of the water-soluble binder and NaCl space holder. The average masses of the samples before and after debinding with standard deviations were 11.47 ± 0.10 g and 8.80 ± 0.11 g, respectively. This resulted in a mass loss of 23.2 ± 0.4%. According to the manufacturer, the weight loss of 316L feedstock during debinding is greater than 3.6 wt%. The calculated mass loss percentage confirmed a complete removal of NaCl spacer and water-soluble binder from the samples.

Carbolite GERO, model HTK 8 MO/16 furnace (Carbolite Gero Ltd., Neuhausen, Germany) was used to sinter the samples using a temperature profile shown in Fig. 1. First, the furnace was heated from room temperature to 200 °C at a heating rate of 180 °C/h (A) followed by holding period of 2 h at 200 °C. Then, heating from 200 °C to 600 °C was carried out at a heating rate of 180 °C/h (B). After a holding period of 2 h at 600 °C, heating to 1360 °C was performed at a heating rate of 300 °C/h (C) followed by a holding period of 2 h at 1360 °C. Finally, cooling down from 1360 °C to 80 °C was performed at a rate of 900 °C/h (D) with a final holding period of 15 min at 80 °C before returning to room temperature.

2.2. Electrodeposition

Electrodeposition of 316L samples was carried out in a simple electrodeposition bath system consisting of a Xantrex XHR 300–3.5 DC power supply (Xantrex Technology, Inc., Burnaby, Canada), a magnetic stirrer, electrolyte in a 250 ml beaker and two electrodes. A two-electrode system was used for simplicity. 25 × 25 mm^2 zinc (thickness of 3.0 mm, >99.99%), copper (thickness of 2.0 mm, >99.99%), and silver (thickness of 2.0 mm, >99.95%) foils were purchased from Goodfellow (Goodfellow Cambridge Limited, Huntingdon, UK) that

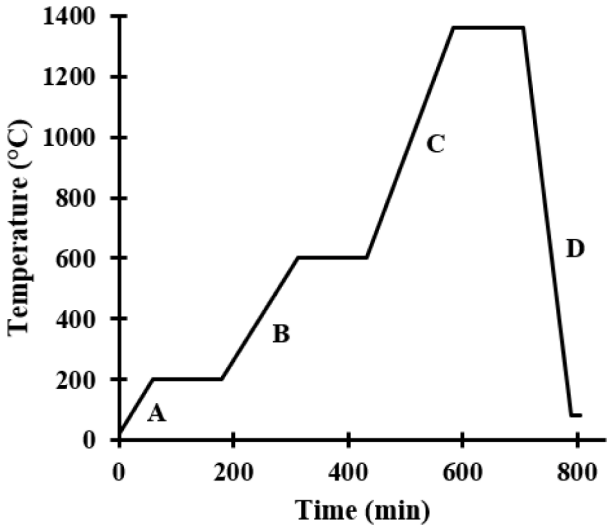

Fig. 1. The sintering cycle of polyMIM® 316L D 120E stainless steel.

Table 1
Typical additives of polyMIM® 316L D 120E as sintered in wt%.

Additive	C	Ni	Cr	Mo	Mn	Si	S	P
wt%	< 0.03	10.0–14.0	16.0–18.5	2.0–3.0	< 2.0	< 1.0	< 0.03	< 0.045

were used as an anode. The sample to be electrodeposited was attached as a cathode to the system. Three different electrolyte compositions were used. The electrolytes were prepared by dissolving the corresponding compounds in 70 ml of deionized water with electrolyte concentration of 0.2 M. Zinc acetate (99.99%, Sigma-Aldrich, Steinheim, Germany) for zinc deposition, copper sulfate (98%, anhydrous, Acros Organics, Geel, Belgium) for copper deposition, and silver nitrate (>99.9%, Apollo Scientific, Bredbury, UK) for silver deposition were used. The power supply was operated in a galvanostatic (i.e., constant current) mode with an electric current of 0.10 A, and a deposition time of 90 min was used. Each sample was weighed before and after electrodeposition to analyze the extent of deposition quantitatively.

2.3. Characterization

A field emission scanning electron microscope (FESEM, Hitachi S-4800, Tokyo, Japan) with energy-dispersive X-ray spectroscopy (EDS) detector was used to investigate and image the sintered porous structures. EDS was used for a detailed elemental information on the deposition of zinc, copper, and silver into the internal pore structure of the samples. Acceleration voltage of 10.0 kV was used with a working distance of 8.0 mm for SEM imaging and 15.0 mm for EDS analysis. The pixel resolution of SEM and EDS images was set to 1280 × 960 and 1024 × 768, respectively.

2.4. Antimicrobial activity testing

Antimicrobial activity testing was carried out using a touch test protocol [26] mimicking bacterial transfer from surfaces. Electrodeposited porous 316L stainless steel structures were studied from *S. aureus* growth inhibition. Three samples of each type were tested to ensure the consistency and repeatability of the results. Together with six non-deposited reference samples (three polished and three unpolished), a total of 24 samples were tested. Bacterial suspension equivalent to the 0.5 McFarland test standard was done on Gram-positive *S. aureus* ATCC 29213. This is equivalent to 1.8×10^8 bacterial colony forming units (CFUs) in a ml of suspension. 50 µl of suspension was applied on the sample surface on which the solution was incubated for 24 h at room temperature. After 24 h a blood agar plate (tryptic soy agar W/5% SB (II); BD, Franklin Lakes, NJ, USA) was brought in contact with the incubated solution for 30 s. After touching, the blood agar plates were incubated at 37 °C for 24 h before calculating the CFUs from these blood agar plates. Antimicrobial activity of the sample surfaces was characterized using the following scale: 0 (no CFUs), 1 (10^3 – 10^4 CFUs), 2 (10^4 – 10^5 CFUs), and 3 (> 10^5 CFUs).

Both porous reference stainless steel samples and porous samples electrodeposited with Zn, Cu, and Ag were tested. Three samples for each metal were tested with the intact metal deposition that covered the whole surface. In addition, the electrodeposited metal was removed from the sample surface by polishing with abrasive paper from three additional samples. After polishing, debris from the abrasive paper was removed from the samples by washing with deionized water and blowing air with pressurized air gun. The polishing removed the metal deposition completely from the sample surface but leaving the deposited metal intact within the pores. Surface polishing was carried out to study if the pores can store sufficient amount of metal for antimicrobial activity against *S. aureus*. For reference, six porous samples were subjected to the antimicrobial testing: three polished surfaces and three unpolished surfaces.

3. Results and discussion

3.1. Morphology of the porous structures

Porous 316L stainless steel specimens were fabricated using NaCl as a space holder material. Controlled removal of NaCl during the debinding process was followed by a formation of pores, which maintained their shape during sintering. The shrinkage of metal materials is an intrinsic property of the sintering process. Thus, the pore size of the sintered porous structures was less than the value predetermined from the NaCl spacer crystal size (200–315 µm).

Fig. 2 shows cross-sectional SEM images of non-porous (a) and porous (b) sintered 316L stainless steel samples. Same injection molding parameters and process steps were used for both samples. The non-porous sample was broken in half mechanically before sintering whereas the porous sample was brittle enough to be broken in half mechanically after sintering.

The inner structure of the non-porous 316L sample did not show any porosity in the cross-sectional fracture surface whereas the internal pore structure of the porous sample consisted of a high number of interconnected pores with a rather uniform shape and size. The average porosity of the porous samples was calculated from the densities of the porous and non-porous samples. Densities were obtained from masses and volumes (calculated from the outer dimensions) of the samples. The average porosity of the porous samples was calculated to be 37.9%.

3.2. Electrodeposition

Each porous 316L sample was weighed before and after the electrodeposition to evaluate the amount of the deposited metal. These masses and the calculated mass of the deposited metal are shown in Table 2.

From Table 2 it can be concluded that there was no significant difference in the amount of deposited zinc and copper. However, the amount of deposited silver was significantly higher. This is due to the difference in electrical conductivity of the used electrolytes and the electrode potentials of the different metals. The comparatively high standard deviation of the deposited mass of silver is partly explained by the poorer adhesion and cohesion of the silver deposition compared to those of zinc and copper deposition.

Porous electrodeposited samples were broken in half mechanically to investigate the zinc, copper, and silver deposits into the internal pore structure of the porous 316L samples. The nature and quantity of the deposition was primarily studied near the sample surface as the deposition on the surface pores are expected to have the largest effect on the antimicrobial activity of the sample.

Fig. 3 shows cross-sectional fracture surface SEM images with two different magnification levels for samples electrodeposited with zinc (a, d), copper (b,e), and silver (c,f) . In the top row images, a single pore is fitted to center of the frame to estimate the overall extent of deposition. It is noteworthy that with all deposited metals, the internal pore structure was not filled with a continuous layer of electrodeposited metals. Instead, the depositions consist of individual flakes of which shape and size depend on the deposited metal. The amount of copper inside the internal pores was higher than for zinc and silver. Silver displayed the lowest deposited amount. The low amount of deposited silver may originate from the tendency of silver to quickly form a thick silver layer on the sample surface during electrodeposition that prevented deposition deeper into the internal pore structure. A better deposition coverage inside the pore structure may be achieved by increasing the overall and surface porosity of the samples by increasing the spacer content during injection molding [27].

On the bottom row, higher magnification SEM images are presented. The silver particles shown in Fig. 3f have generally a smaller size than their zinc (d) and copper (e) counterparts. The deposition pattern was rather similar for zinc and copper, although copper flakes have a more defined, leaf-like structure.

Copper deposition into the internal pore structure of porous 316L stainless steel was analyzed in Fig. 4. Fig. 4a and Fig. 4b were captured near the surface of the sample similar to Fig. 3. These images display the highest coverage of copper found inside the pore structure. The whole metal surface was covered with copper deposition. However, individual

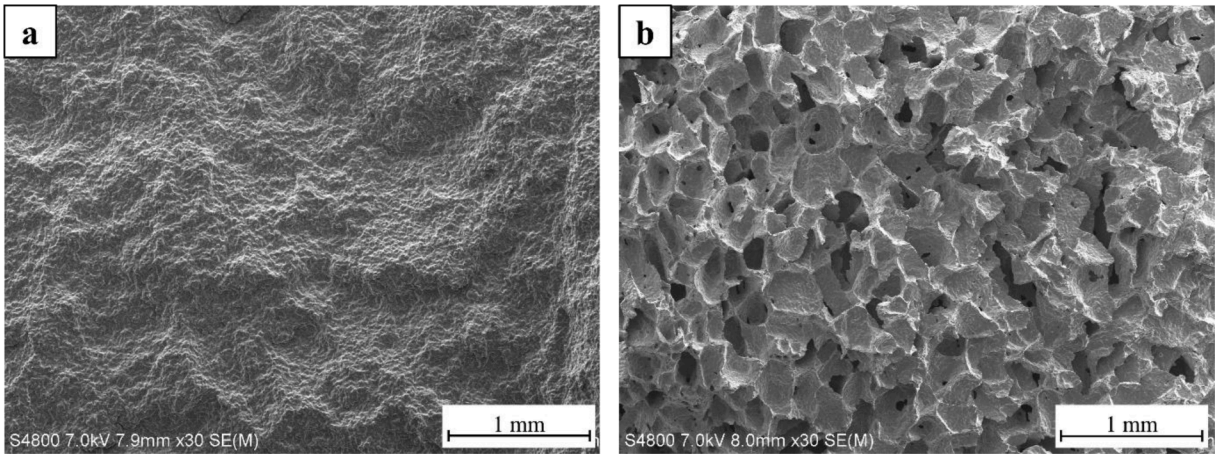

Fig. 2. Cross-sectional low-magnification (×30) SEM images of the structure of a) non-porous and b) porous (20 wt% NaCl) sintered 316L stainless steel samples.

Table 2
Average masses of the porous 316L samples before and after electrodeposition and the mass of the deposited metal with standard deviations.

Deposited metal	Before deposition (g)	After deposition (g)	Deposited mass (g)
Zn	8.41 ± 0.14	8.58 ± 0.12	0.17 ± 0.03
Cu	8.41 ± 0.07	8.59 ± 0.07	0.19 ± 0.00
Ag	8.38 ± 0.07	8.74 ± 0.13	0.37 ± 0.11

copper flakes with their distinctive shapes can be distinguished from the deposition (4b). It is worth emphasizing that the regional variation of copper deposition was rather high, even in the case of pores near the sample surface. This can be explained by the irregularity of pore structure: some internal pores were directly connected to surface pores, whereas the other pores were more closed or had smaller openings to the sample surface.

EDS line scan analysis was used to confirm that the investigated particles were copper. The analyses are presented as subfigures on the top right corners of Fig. 4a and Fig. 4b. Magnification levels of 3 kX and 10 kX were used for the EDS analysis, respectively. The line scan displays the amount of copper detected on the path of the yellow arrow and draws a blue-colored spectrum based on the detected copper counts. In both analyses high copper peaks were detected that coincided with the light-colored crystals in the SEM images. This confirms that the crystals were copper. Zinc and silver particles inside the pore structure were confirmed by a similar EDS analysis. The EDS analysis figure presented in Fig. 4a shows an occasional tendency of copper to deposit in bigger spheric clusters. Similar deposition pattern was not observed with zinc and silver.

Fig. 5 shows SEM images of the sample surface after the copper electrodeposition. Here the sample was attached to the electrodeposition system in such a way that a small part of the sample surface was not deposited with copper. This allows the difference between copper-deposited surface and non-deposited surface to be imaged in one image using SEM. In Fig. 5a the part of the sample in the lower half of the image was deposited with copper, while the upper half was not deposited.

Fig. 5b shows exactly the same part of the sample surface but here the electrodeposited copper was removed by polishing the sample surface with abrasive paper followed by cleaning and drying. The lower half of the image was originally deposited with copper. It can be concluded that

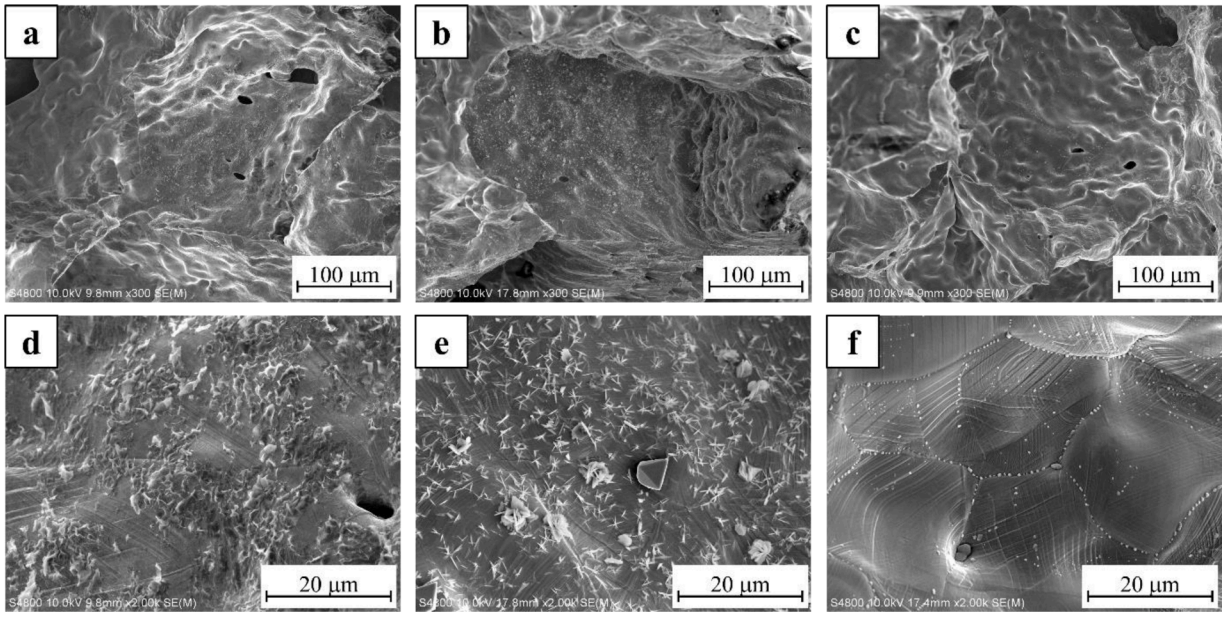

Fig. 3. SEM images with two different magnification levels (×300 for the top row and ×2.0 k for the bottom row) of metal electrodeposition into the internal pore structure of the sintered porous 316L stainless steel. The deposited metals from left to right are zinc (a, d), copper (b,e), and silver (c,f).

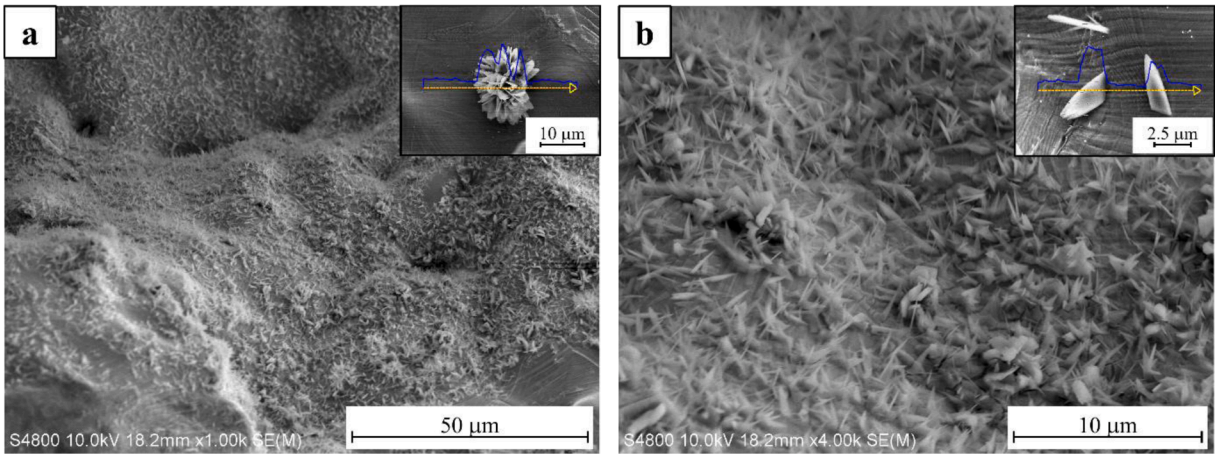

Fig. 4. High-magnification (×1.0 k and ×4.0 k) SEM images of copper electrodeposition into the internal pore structure of the sintered porous 316L stainless steel. In subfigures smaller SEM images are displayed with an EDS line scan (yellow arrow) analysis displaying the graph for copper content (blue spectrum in subfigures).

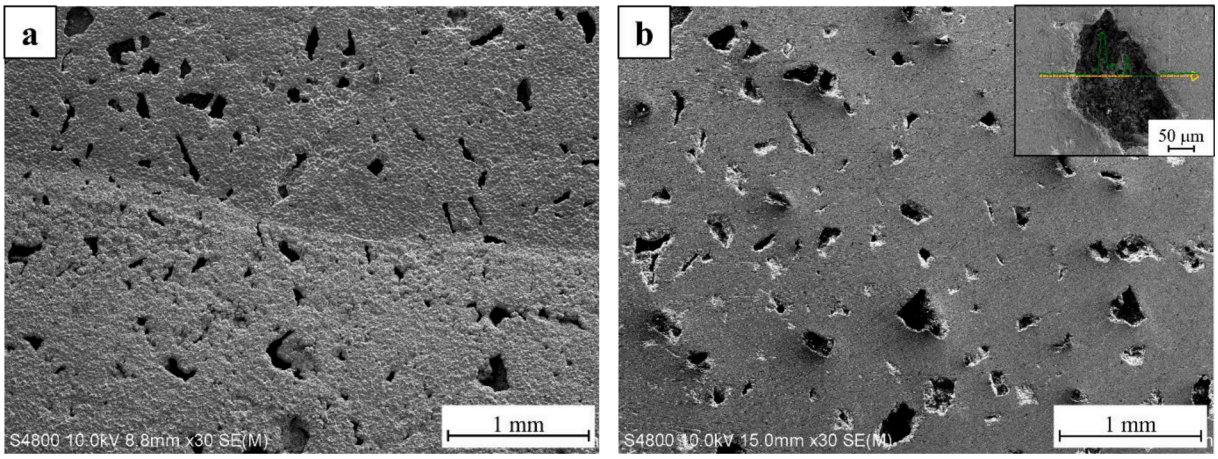

Fig. 5. Low-magnification (×30) SEM images of copper electrodeposited porous 316L sample surface before (a) and after (b) the removal of surface copper deposition by polishing. In subfigure an EDS line scan analysis displays the copper content inside a single surface pore.

polishing fully removed the copper from the sample surface. In addition, no difference in surface morphology was present between the deposited (lower half) and non-deposited (upper half) parts of the polished sample surface. It was also evident that polishing exposed the surface pores under the copper deposition. Subfigure in Fig. 5b contains an EDS line scan analysis from a sample surface after copper was removed by polishing. In the analysis, a line scan was measured across a single pore located on the surface previously deposited with copper. The green graph represents the amount of copper present in each spot along the path depicted by the yellow arrow. The analysis confirmed that no copper was left on the surface surrounding the pore, while there was still copper left inside the pore as displayed by a higher green peak intensity in the middle of the graph coinciding with the pore.

3.3. Antimicrobial activity

Fig. 6 shows the *S. aureus* growth after 24 h incubation on sample surface with the corresponding blood agar plates on top. Each bar shows the average of the test results of the three similar test samples. The unpolished reference stainless steel sample had no antimicrobial effect on the growth of *S. aureus*, and a significant number of colonies were formed on the blood agar plate. Polishing of the reference stainless steel sample resulted in a minor reduction of bacterial growth: two samples had a value of 1 whereas the third had a value of 3 resulting in an average value of 1.67 with a standard deviation of 1.15. The agar plate shown above the polished reference bar displays a growth value of 1 with three bacterial colonies.

All electrodeposited samples completely prevented the growth of *S. aureus*. This was expected with all unpolished samples on which a relatively thick metal layer was covering the stainless steel surface. In addition, the polished electrodeposited sample surfaces inhibited bacterial growth equally well. These test results confirm that deposition of zinc, copper, and silver particles into the pores of 316L stainless steel is sufficient for the efficient antimicrobial activity.

It can be concluded that no covering layer of metal is required on the sample surface since the pores can sufficiently store the antimicrobial agents. It is noteworthy that the small particles visible on the unpolished silver-deposited sample (second from right) are not bacterial colonies, but silver particles attached from the deposited sample surface during the touching face i.e. the adhesion of silver particles was poor to the stainless steel and they are easily removed from the unpolished surface. It is also worth emphasizing that hemolysis visible on some of blood agar plates (fifth and eighth agar plate from the left) was caused by the corresponding metals from the unpolished copper and polished silver samples.

4. Conclusions

Porous injection molded 316L stainless steel samples were fabricated by MIM using the PSH technique. These sintered porous samples were

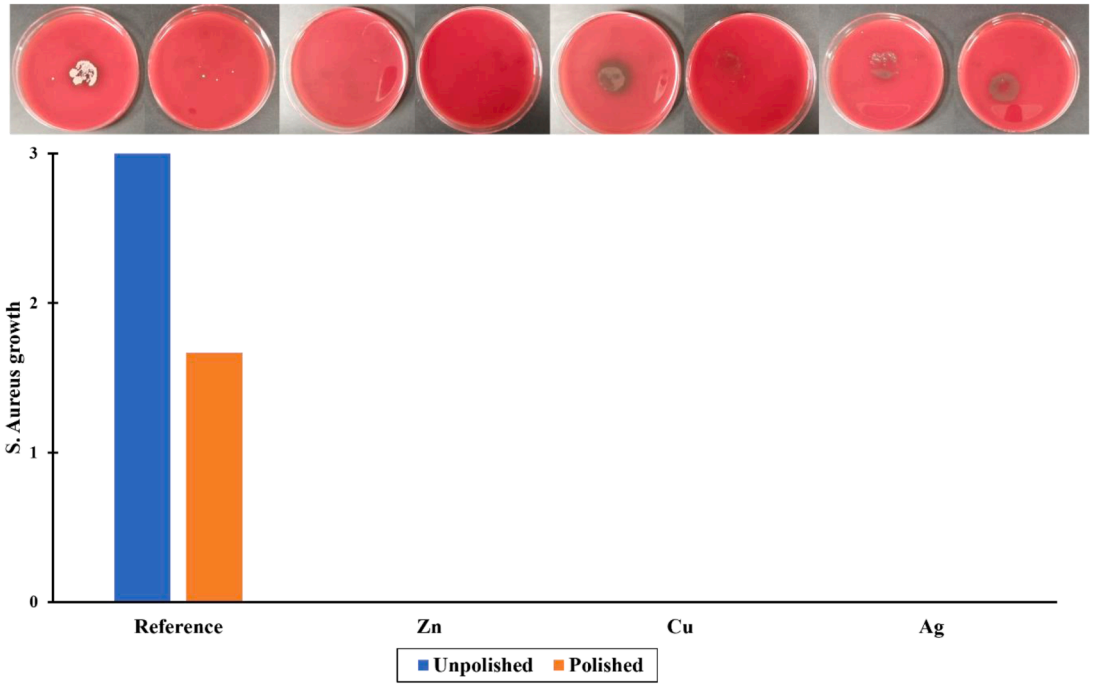

Fig. 6. Growth of S. aureus on the porous 316L sample surfaces after 24 h incubation. No growth was observed in all electrodeposited samples and the corresponding agar plates are shown on top.

electrodeposited with zinc, copper, and silver that was characterized with SEM and EDS. The antimicrobial activity of the porous electrodeposited samples was investigated with a touch test using gram-positive *S. aureus* bacteria mimicking bacterial transfer from surfaces that is of paramount importance, for example, in hospital settings.

Our results showed that electrodeposition improved the antimicrobial activity of the porous 316L stainless steel structures. Electrodeposited metal layer was removed from the sample surfaces by polishing that left metal only within the pores of the sample. It was confirmed that metal deposited within the pores was sufficient to completely inhibit the growth of *S. aureus* equally to a continuous electrodeposited coating on the sample surface. The results obtained in this study can be used to improve the antimicrobial activity of stainless steel materials without a need to apply continuous coating on their surface. Hence, effective antimicrobial properties can be achieved using significantly less material followed by reduced material costs. On the contrary, many fabrication steps required during the electrodeposition may limit applicability in practical and commercial use. However, deposition within the pores provides protection against mechanical wear that is expected to prolong the lifetime of the activity.

Author statement

All authors have gone through the changes in the revised manuscript and accept the submission on the revised version. The author contributions are declared at the end of the revised manuscript

Data availability

The data presented in this study are available in article here. The data presented in this study are also available upon request from the corresponding author.

CRediT authorship contribution statement

Matti Kultamaa: Investigation, Writing – original draft. **Marianne Gunell:** Investigation. **Kari Mönkkönen:** Conceptualization, Funding acquisition, Project administration, Resources. **Mika Suvanto:** Conceptualization, Funding acquisition, Project administration, Resources, Supervision, Writing – review & editing. **Jarkko J. Saarinen:** Conceptualization, Project administration, Supervision, Writing – review & editing.

Declaration of Competing Interest

The authors declare that they have no known competing financial interests or personal relationships that could have appeared to influence the work reported in this paper.

Data availability

Data will be made available on request.

Acknowledgments

We gratefully acknowledge the Business Finland/ERDF (European Regional Development Fund) project “MIM Components for Harsh Conditions” (Grant agreement 7929/31/2019) for financial support. M. Kultamaa acknowledges the Finnish Cultural Foundation, North Karelia Regional fund for financial support. JJS acknowledges the Academy of Finland funding (339544) and the Academy of Finland Flagship for Photonics Research and Innovation (PREIN, decision no. 320166).

References

[1] S. Dwivedi, A. Rai Dixit, A. Kumar Das, Wetting behavior of selective laser melted (SLM) bio-medical grade stainless steel 316L, Mater. Today Proc. 56 (2021) 46–50, https://doi.org/10.1016/j.matpr.2021.12.046.

[2] S. Sathishkumar, C. Sridevi, R. Rajavel, P. Karthikeyan, Smart flower like MgO/Tb, Eu-substituted hydroxyapatite dual layer coating on 316L SS for enhanced corrosion resistance, antibacterial activity and osteocompatibility, J. Sci. Adv. Mater. Devices 5 (2020) 545–553, https://doi.org/10.1016/j.jsamd.2020.09.007.

[3] R. Alias, R. Mahmoodian, K. Genasan, K.M. Vellasamy, M. Hamdi Abd Shukor, T. Kamarul, Mechanical, antibacterial, and biocompatibility mechanism of PVD grown silver–tantalum-oxide-based nanostructured thin film on stainless steel 316L

for surgical applications, Mater. Sci. Eng. C 107 (2020), 110304, https://doi.org/10.1016/j.msec.2019.110304.
[4] G. Gao, Z. Zhang, Cavitation erosion behavior of 316L stainless steel, Tribol. Lett. 67 (2019) 1–12, https://doi.org/10.1007/s11249-019-1225-0.
[5] Q. Chen, G.A. Thouas, Metallic implant biomaterials, Mater. Sci. Eng. R Rep. 87 (2015) 1–57, https://doi.org/10.1016/j.mser.2014.10.001.
[6] N. Ciacotich, R.U. Din, J.J. Sloth, P. Møller, L. Gram, An electroplated copper–silver alloy as antibacterial coating on stainless steel, Surf. Coat. Technol. 345 (2018) 96–104, https://doi.org/10.1016/j.surfcoat.2018.04.007.
[7] J.M. Boyce, Environmental contamination makes an important contribution to hospital infection, J. Hosp. Infect. 65 (2007) 50–54, https://doi.org/10.1016/S0195-6701(07)60015-2.
[8] T.S. Awad, D. Asker, B.D. Hatton, Food-safe modification of stainless steel food-processing surfaces to reduce bacterial biofilms, ACS Appl. Mater. Interfaces 10 (2018) 22902–22912, https://doi.org/10.1021/acsami.8b03788.
[9] K. Hori, S. Matsumoto, Bacterial adhesion: from mechanism to control, Biochem. Eng. J. 48 (2010) 424–434, https://doi.org/10.1016/j.bej.2009.11.014.
[10] A.C.M. Miranda, L.C.A. Barbosa, M.A. Masood, J.O.S. Varejao, M. Sordi, C.A. M. Benfatti, A.L. Pimenta, Inhibitory effect on biofilm formation of pathogenic bacteria induced by rubrolide lactam analogues, ACS Omega 3 (2018) 18475–18480, https://doi.org/10.1021/acsomega.8b02334.
[11] M. Rizwan, R. Alias, U.Z. Zaidi, R. Mahmoodian, M. Hamdi, Surface modification of valve metals using plasma electrolytic oxidation for antibacterial applications: a review, J. Biomed. Mater. Res. - Part A 106 (2018) 590–605, https://doi.org/10.1002/jbm.a.36259.
[12] F.G. Echeverrigaray, S. Echeverrigaray, A.P.L. Delamare, C.H. Wanke, C. A. Figueroa, I.J.R. Baumvol, C. Aguzzoli, Antibacterial properties obtained by low-energy silver implantation in stainless steel surfaces, Surf. Coat. Technol. 307 (2016) 345–351, https://doi.org/10.1016/j.surfcoat.2016.09.005.
[13] M. Geetha, A.K. Singh, R. Asokamani, A.K. Gogia, Ti based biomaterials, the ultimate choice for orthopaedic implants - a review, Prog. Mater. Sci. 54 (2009) 397–425, https://doi.org/10.1016/j.pmatsci.2008.06.004.
[14] G. Ryan, A. Pandit, D.P. Apatsidis, Fabrication methods of porous metals for use in orthopaedic applications, Biomaterials 27 (2006) 2651–2670, https://doi.org/10.1016/j.biomaterials.2005.12.002.
[15] K. Nishiyabu, S. Matsuzaki, S. Tanaka, Fabrication of micro porous metal components by metal injection molding based powder space holder method, High Temp. Mater. Process. 26 (2007) 257–267, https://doi.org/10.1515/HTMP.2007.26.4.257.
[16] H.Ö. Gülsoy, R.M. German, Production of micro-porous austenitic stainless steel by powder injection molding, Scr. Mater. 58 (2008) 295–298, https://doi.org/10.1016/j.scriptamat.2007.10.004.
[17] A. Manonukul, N. Muenya, F. Léaux, S. Amaranan, Effects of replacing metal powder with powder space holder on metal foam produced by metal injection moulding, J. Mater. Process. Technol. 210 (2010) 529–535, https://doi.org/10.1016/j.jmatprotec.2009.10.016.
[18] J.T. Seil, T.J. Webster, Antimicrobial applications of nanotechnology: methods and literature, Int. J. Nanomed. 7 (2012) 2767–2781, https://doi.org/10.2147/IJN.S24805.
[19] M. Schlesinger, Electroless and electrodeposition of silver, Eds., in: M. Schlesinger, M. Paunovic (Eds.), Modern Electroplating, 5th ed., John Wiley & Sons, Hoboken, 2014, pp. 131–138, https://doi.org/10.1002/9780470602638.ch5. Incorporated
[20] R. Winand, Electrodeposition of zinc and zinc alloys, Eds., in: M. Schlesinger, M. Paunovic (Eds.), Modern Electroplating, 5th ed., John Wiley & Sons, Hoboken, 2014, pp. 285–307, https://doi.org/10.1002/9780470602638.ch10. Incorporated
[21] J.W. Dini, D.D. Snyder, Electrodeposition of copper, Eds., in: M. Schlesinger, M. Paunovic (Eds.), Modern Electroplating, 5th ed., John Wiley & Sons, Hoboken, 2014, pp. 33–78, https://doi.org/10.1002/9780470602638.ch2. Incorporated
[22] Y. Reyes-Vidal, R. Suarez-Rojas, C. Ruiz, J. Torres, Ş. Ţălu, A. Méndez, G. Trejo, Electrodeposition, characterization, and antibacterial activity of zinc/silver particle composite coatings, Appl. Surf. Sci. 342 (2015) 34–41, https://doi.org/10.1016/j.apsusc.2015.03.037.
[23] A. Méndez-Albores, S.G. González-Arellano, Y. Reyes-Vidal, J. Torres, Ş. Ţălu, B. Cercado, G. Trejo, Electrodeposited chrome/silver nanoparticle (Cr/AgNPs) composite coatings: characterization and antibacterial activity, J. Alloys Compd. 710 (2017) 302–311, https://doi.org/10.1016/j.jallcom.2017.03.226.
[24] M. Silva-Ichante, Y. Reyes-Vidal, F.J. Bácame-Valenzuela, J.C. Ballesteros, E. Arciga, Ş. Ţălu, A. Méndez-Albores, G. Trejo, Electrodeposition of antibacterial Zn-Cu/silver nanoparticle (AgNP) composite coatings from an alkaline solution containing glycine and AgNPs, J. Electroanal. Chem. 823 (2018) 328–334, https://doi.org/10.1016/j.jelechem.2018.06.032.
[25] Y. Qing, K. Li, D. Li, Y. Qin, Antibacterial effects of silver incorporated zeolite coatings on 3D printed porous stainless steels, Mater. Sci. Eng. C 108 (2020), 110430, https://doi.org/10.1016/j.msec.2019.110430.
[26] M. Gunell, J. Haapanen, K.J. Brobbey, J.J. Saarinen, M. Toivakka, J.M. Mäkelä, P. Huovinen, E. Eerola, Antimicrobial characterization of silver nanoparticle-coated surfaces by “touch test” method, Nanotechnol. Sci. Appl. 10 (2017) 137–145, https://doi.org/10.2147/NSA.S139505.
[27] M. Kultamaa, K. Mönkkönen, J.J. Saarinen, M. Suvanto, Corrosion protection of injection molded porous 440c stainless steel by electroplated zinc coating, Coatings 11 (2021) 1–11, https://doi.org/10.3390/coatings11080949.